

Optical signature of flat bands in topological hourglass semimetal Nb_3SiTe_6

Shize Cao(曹仕泽), Cuiwei Zhang(张翠伟), Yueshan Xu(徐越山), Jianzhou Zhao(赵建洲), Youguo Shi(石友国), Yun-Ze Long(龙云泽), Jianlin Luo(雒建林), and Zhi-Guo Chen(谌志国)

Citation: Chin. Phys. B, 2025, 34 (**2**): 027101. DOI: 10.1088/1674-1056/ad9e9c
Journal homepage: http://cpb.iphy.ac.cn; http://iopscience.iop.org/cpb

What follows is a list of articles you may be interested in

Electronic band structures of topological kagome materials

Man Li(李满), Huan Ma(马欢), Rui Lou(娄睿), and Shancai Wang(王善才)
Chin. Phys. B, 2025, 34 (**1**): 017101. DOI: 10.1088/1674-1056/ad925d

Visualizing the electronic structure of kagome magnet $LuMn_6Sn_6$ by angle-resolved photoemission spectroscopy

Man Li(李满), Qi Wang(王琦), Liqin Zhou(周丽琴), Wenhua Song(宋文华), Huan Ma(马欢), Pengfei Ding(丁鹏飞), Alexander Fedorov, Yaobo Huang(黄耀波), Bernd Büchner, Hechang Lei(雷和畅), Shancai Wang(王善才), and Rui Lou(娄睿)
Chin. Phys. B, 2024, 33 (**11**): 117101. DOI: 10.1088/1674-1056/ad7afe

Layered kagome compound $Na_2Ni_3S_4$ with topological flat band

Junyao Ye(叶君耀), Yihao Lin(林益浩), Haozhe Wang(王浩哲), Zhida Song(宋志达), Ji Feng(冯济), Weiwei Xie(谢韦伟), and Shuang Jia(贾爽)
Chin. Phys. B, 2024, 33 (**5**): 057103. DOI: 10.1088/1674-1056/ad3431

Band structures of strained kagome lattices

Luting Xu(徐露婷) and Fan Yang(杨帆)
Chin. Phys. B, 2024, 33 (**2**): 027101. DOI: 10.1088/1674-1056/ad0291

Flat band in hole-doped transition metal dichalcogenide observed by angle-resolved photoemission spectroscopy

Zilu Wang(王子禄), Haoyu Dong(董皓宇), Weichang Zhou(周伟昌), Zhihai Cheng(程志海), and Shancai Wang(王善才)
Chin. Phys. B, 2023, 32 (**6**): 067103. DOI: 10.1088/1674-1056/acc7f9

Optical signature of flat bands in topological hourglass semimetal Nb_3SiTe_6

Shize Cao(曹仕泽)[1,2,†], Cuiwei Zhang(张翠伟)[2,†], Yueshan Xu(徐越山)[2,†], Jianzhou Zhao(赵建洲)[3,‡], Youguo Shi(石友国)[2,4], Yun-Ze Long(龙云泽)[1,§], Jianlin Luo(雒建林)[2,4], and Zhi-Guo Chen(谌志国)[2,4,¶]

[1] *Collaborative Innovation Center for Nanomaterials & Devices, College of Physics, Qingdao University, Qingdao* 266071, *China*
[2] *Beijing National Laboratory for Condensed Matter Physics, Institute of Physics, Chinese Academy of Sciences, Beijing* 100190, *China*
[3] *Co-Innovation Center for New Energetic Materials, Southwest University of Science and Technology, Mianyang* 621010, *China*
[4] *Songshan Lake Materials Laboratory, Dongguan* 523808, *China*

(Received 3 November 2024; revised manuscript received 12 December 2024; accepted manuscript online 13 December 2024)

Flat electronic bands in condensed matter provide a rich avenue for exploring novel quantum phenomena. Here, we report an optical spectroscopy study of a topological hourglass semimetal Nb_3SiTe_6 with the electric field of the incident light parallel to its crystalline *ab*-plane. The *ab*-plane optical conductivity spectra of Nb_3SiTe_6 single crystals exhibit a remarkable peak-like feature around 1.20 eV, which is mainly contributed by the direct optical transitions between the two *ab-initio*-calculation-derived flat bands along the momentum direction *Z*–*U*. Our results pave the way for investigating exotic quantum phenomena based on the flat bands in topological hourglass semimetals.

Keywords: flat band, topological semimetal, optical spectroscopy

PACS: 71.20.–b, 73.21.–b, 78.30.–j, 78.67.–n

DOI: 10.1088/1674-1056/ad9e9c **CSTR:** 32038.14.CPB.ad9e9c

1. Introduction

Flat electronic bands, which represent dispersionless bands with divergent density of state (DOS), have been attracting great interest in condensed matter community due to their crucial roles in the emergence of various quantum phenomena, such as fractional quantum Hall effect,[1–5] superconductivity,[6–13] and ferromagnetism.[14–20] Several electron systems, including kagome-lattice compounds,[21–41] twisted bilayer graphene,[42] Weyl semimetals,[43–46] and heavy-fermion materials,[47] possess flat electronic bands.[48–50] An important question is whether flat bands can be observed in a broader class of electron systems.

A van der Waals material Nb_3SiTe_6 shows a topological hourglass semimetal phase with the hourglass-type band structure protected by the nonsymmorphic space group symmetry.[51–53] Furthermore, the signatures of weak topological insulator were identified in Nb_3SiTe_6.[54] Electrical transport study indicates that electron coherence is unexpectedly enhanced in few-layer Nb_3SiTe_6 owing to the quantum-confinement-induced suppression of electron–phonon interactions.[55] Moreover, Nb_3SiTe_6 thin flakes exhibit Shubnikov–de Haas oscillations with nontrivial π-Berry phase,[56] which implies the nontrivial topological nature of its electronic bands. It was theoretically predicted that the Berry curvature dipole in Nb_3SiTe_6 should produce nonlinear Hall effect.[57] Additionally, the device made of Nb_3SiTe_6 has a quite high thermoelectric power and a very large power factor.[58] Recently, linearly polarized infrared spectroscopy measurements of Nb_3SiTe_6 show the excitations around 0.15 eV and 0.28 eV,[59] which were ascribed to the fingerprints of van Hove singularities in its electronic band structure. However, the optical signature of the flat bands in Nb_3SiTe_6 has rarely been observed in experiments.

Optical spectroscopy is an efficient experimental technique for probing interband transitions from occupied to empty states[60–64] and thus enables us to search for the optical signature of the flat electronic bands in Nb_3SiTe_6. Here, we present the optical reflectance measurements of the Nb_3SiTe_6 single crystals over broad photon energies with the directions of the electric fields of the incident light parallel to the newly cleaved surfaces (i.e., crystalline *ab*-plane with the in-plane lattice parameters $a = 11.5$ Å and $b = 6.3$ Å). Our optical reflectance measurements reveal a remarkable peak-like feature around 1.20 eV in the real part (i.e., $\sigma_1(\omega)$) of the optical conductivity spectra which are induced by the electric fields of the incident light parallel to the *ab*-plane of Nb_3SiTe_6. Moreover, two flat bands obtained by *ab-initio* calculations are separately located at -0.21 eV and 0.99 eV along the momentum direction *Z*–*U* and have the energy distance ~ 1.20 eV, which is consistent with the energy position of the remarkable

[†]These authors contributed equally to this work.
[‡]Corresponding author. E-mail: jzzhao@swust.edu.cn
[§]Corresponding author. E-mail: yunze.long@qdu.edu.cn
[¶]Corresponding author. E-mail: zgchen@iphy.ac.cn

© 2025 Chinese Physical Society and IOP Publishing Ltd. All rights, including for text and data mining, AI training, and similar technologies, are reserved.

peak-like feature around 1.20 eV. Thus, the peak-like feature around 1.20 eV in the $\sigma_1(\omega)$, which arises primarily from the direct optical transitions between the two flat bands along Z–U, can be assigned as an optical signature of the flat bands in Nb_3SiTe_6.

2. Results and discussion

The Nb_3SiTe_6 single crystals were grown by a chemical vapor transport method.[55] High-purity elemental Nb, Si, and Te with a molar ratio of 3:2:6 were put into a quartz tube under high vacuum. The quartz tube was placed in the two-zone furnace where the temperatures of the hot and cool sides were set as 1223 K and 1123 K, respectively.

The optical reflectance measurements in the temperature range from 300 K to 8 K were performed on a Bruker Vertex 80V Fourier transform spectrometer. The reflectance spectra (i.e., $R(\omega)$) of the freshly cleaved *ab*-plane of the Nb_3SiTe_6 single crystals were obtained using an *in-situ* gold and aluminum overcoating technique. The Kramers–Kronig transformation of the $R(\omega)$ was used to get the $\sigma_1(\omega)$ of Nb_3SiTe_6.

Figure 1(a) displays the *ab*-plane $R(\omega)$ of the Nb_3SiTe_6 single crystals at two typical temperatures $T = 8$ K and 300 K in the energy range up to 2 eV. As shown in the inset of Fig. 1(a), the $R(\omega)$ at $T = 8$ K at energies lower than 30 meV is higher than that at $T = 300$ K and approaches to unity, which exhibits a good metallic response. Besides the metallic optical response at low energies, several hump-like features can be clearly observed at high energies in the $R(\omega)$ at $T = 8$ K.

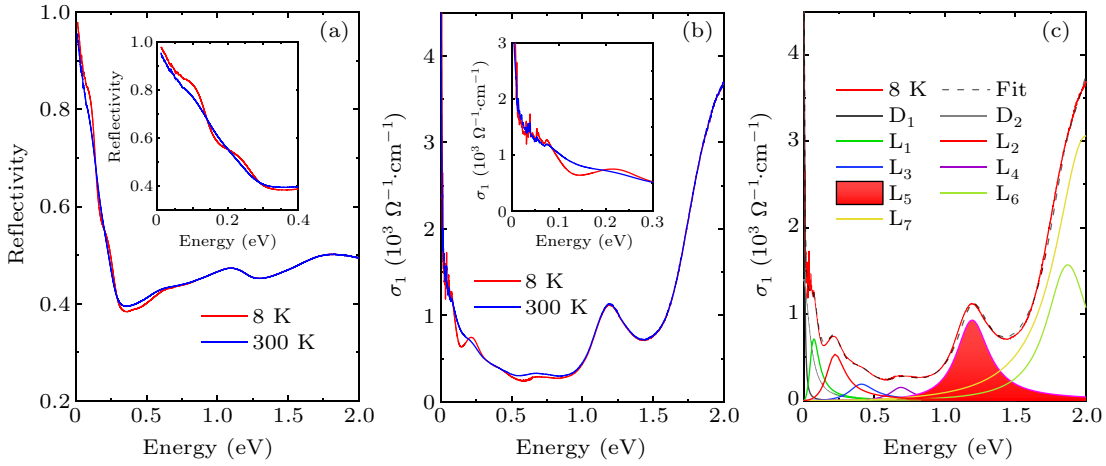


Fig. 1. (a) Reflectance spectra of Nb_3SiTe_6 measured with the electric field of the incident light parallel to the crystalline *ab*-plane at two typical temperatures $T = 8$ K and 300 K in the energy range up to 2 eV. The inset in (a) shows the reflectance spectra in the energy range up to 0.4 eV. (b) Real part $\sigma_1(\omega)$ of the *ab*-plane optical conductivity of Nb_3SiTe_6 at two typical temperatures $T = 8$ K and 300 K in the energy range up to 2 eV. The inset in (b) displays the $\sigma_1(\omega)$ in the energy range up to 0.4 eV. (c) Drude–Lorentz fit to the *ab*-plane $\sigma_1(\omega)$ of Nb_3SiTe_6 at $T = 8$ K. D_1 and D_2 represent the two Drude components. L_1–L_7 are the Lorentzian components. The Lorentzian component L_5 shaded in red color indicates the distinct peak-like feature around 1.20 eV.

To study the nature of the hump-like features present in the $R(\omega)$ of Nb_3SiTe_6, we obtained the $\sigma_1(\omega)$ by the Kramers–Kronig transformation of the $R(\omega)$. Figure 1(b) depicts the $\sigma_1(\omega)$ at $T = 8$ K and 300 K. In the inset of Fig. 1(b), upturn-like features (Drude components) coming from the optical response of the free carriers can be observed at energies lower than 50 meV in the $\sigma_1(\omega)$ at $T = 8$ K and 300 K, respectively, which is in agreement with the metallic behavior of the $R(\omega)$. Moreover, corresponding to the hump-like features in the $R(\omega)$, a series of peak-like features are present in the $\sigma_1(\omega)$.

To identify the energy positions of the peak-like features in Fig. 1, we fit the $\sigma_1(\omega)$ based on a standard Drude–Lorentz model

$$\sigma_1 = \frac{2\pi}{Z_0}\frac{\omega_D^2\Gamma_D}{\omega^2+\Gamma_D^2} + \sum_j \frac{2\pi}{Z_0}\frac{S_j^2\omega^2\Gamma_j}{(\omega_j^2-\omega^2)^2+\omega^2\Gamma_j^2}, \quad (1)$$

where $Z_0 = 377\ \Omega$ is the electric impedance, ω_D and Γ_D are the plasma energy and the relaxation rate of free carriers, respectively, while ω_j, S_j, and Γ_j are the resonance energy, the mode strength and the damping of each Lorentzian term, respectively. The first term in Eq. (1) represents the Drude component. The rest of the terms in Eq. (1) are the Lorentzian components which can be used to describe the optical responses of interband transitions. Figure 1(c) displays the Drude–Lorentz fit to the $\sigma_1(\omega)$ at $T = 8$ K (see the fitting parameters in Table 1). Therein, the energy positions (i.e., 0.22 eV, 0.41 eV, and 2.13 eV) of the Lorentzian peaks L_2, L_3 and L_7 are close to those (i.e., 0.28 eV, 0.41 eV, and 2.00 eV) of the Lorentzian peaks previously measured by linearly polarized infrared spectroscopy. It is worth noticing that a remarkable peak-like feature, which was fitted by the Lorentzian peak L_5 shaded in red color, appears around 1.20 eV in Fig. 1(c). However, the peak-like feature around 1.20 eV in the $\sigma_1(\omega)$ obtained by our optical reflectance measurements cannot be well resolved in the previously reported $\sigma_1(\omega)$ obtained by linearly polarized infrared spectroscopy. The electric fields ($\boldsymbol{E}\|ab$-plane)

of the incident light utilized in our optical reflectance study not only can excite the inter-band transitions coupled with the electric fields ($\boldsymbol{E}\|a$-axis and $\boldsymbol{E}\|b$-axis) of the incident light used in the previously linearly polarized infrared study but also can induce the inter-band transitions coupled with the electric fields of the incident light with the direction between the a-axis and the b-axis. Thus, the peak-like feature around 1.20 eV in the $\sigma_1(\omega)$ obtained by our optical reflectance measurements, which is invisible in the previously reported $\sigma_1(\omega)$, may arise from the inter-band transitions coupled with the electric fields of the incident light with the directions between the a-axis and the b-axis.

Table 1. Parameters of the Drude–Lorentz fit to the $\sigma_1(\omega)$ at $T = 8$ K.

j	ω_j (meV)	Γ_j (meV)	S_j (meV)	$\omega_{\rm D}$ (meV)	$\Gamma_{\rm D}$ (meV)
D_1	–	–	–	600	46
D_2	–	–	–	800	53
L_1	74	82	710	–	–
L_2	224	160	860	–	–
L_3	410	82	600	–	–
L_4	700	190	500	–	–
L_5	1200	280	1465	–	–
L_6	1860	312	2240	–	–
L_7	2130	580	3770	–	–

We checked whether the peak-like feature around 1.20 eV is intimately associated with the optical absorptions of excitons and polarons. The Drude–Lorentz fit to the $\sigma_1(\omega)$ at $T = 8$ K indicates that the plasma energy of the total free charge carriers in Nb_3SiTe_6 $\omega_{\rm D}^{\rm T} = \sqrt{\omega_{\rm D1}^2 + \omega_{\rm D1}^2} = 1000$ meV, which is higher than those in some good metals such as $Co_3Sn_2S_2$ with $\omega_{\rm D} = 258$ meV,[61] and $BaFe_2As_2$ with $\omega_{\rm D} = 582$ meV.[62–64] It is well known that in good metals, the high concentration of free charge carriers means a significant screening of the Coulomb interactions between the electron and hole of an exciton, which leads to the absence of the excitonic feature. Thus, the peak-like feature around 1.20 eV in the $\sigma_1(\omega)$ of Nb_3SiTe_6 with the high charge carrier density and the significant Coulomb screening is unlikely to arise from an exciton absorption.[65–70] Furthermore, it was reported that if the plasma energy is not higher than the longitudinal-optical-phonon energy, the longitudinal-optical phonon would be insufficiently screened by charge free carriers, which results in the observation of the polaron feature.[71–73] However, the large plasma energy (i.e., 1000 meV) in Nb_3SiTe_6 is generally higher than the longitudinal-optical phonon in this topological hourglass semimetal, which indicates that the longitudinal-optical phonon in Nb_3SiTe_6 should be significantly screened by the charge free carriers and suggests that the peak-like feature around 1.20 eV should not come from a polaron absorption.

To identify the origin of the peak-like feature around 1.20 eV in the $\sigma_1(\omega)$ here, we performed *ab-initio* calculations on the electronic band structure and DOS of Nb_3SiTe_6. The electronic band structure of Nb_3SiTe_6 was calculated via the density functional theory, within the generalized gradient approximation (GGA) of Perdew–Burke–Ernzerhof (PBE) realization, as implemented in the Vienna *ab initio* Simulation Package (VASP). The projector augmented wave (PAW) pseudopotentials were adopted for the calculations. Electrons belonging to the outer atomic configuration were treated as valence electrons, here corresponding to 11 electrons in Nb ($4p^6 4d^4 5s^1$), 6 electrons in Te ($5s^2 5p^4$) and 4 electrons in Si ($3s^2 3p^2$). The kinetic energy cutoff was fixed to 400 eV, and a Γ-center grid of $5 \times 10 \times 4$ k-points was adopted for self-consistency. The energy convergence accuracy was set to 10^{-7} eV.

Figure 2(a) displays the calculated electronic bands along high symmetry directions in the energy range from -1.40 eV to 1.40 eV. It is worth noticing that along the momentum direction Z–U, two flat bands indicated by the red lines in Fig. 2(a) are located at -0.21 eV and 0.99 eV, respectively. The energy distance of these two flat bands is ~ 1.20 eV, which is consistent with the energy position of the remarkable peak-like feature around 1.20 eV in the $\sigma_1(\omega)$. Moreover, figure 2(b) shows that the calculated DOS has two peaks indicated by the red stars at the energy positions (i.e., -0.21 eV and 0.99 eV) of the two flat bands. Although the DOS peak at 0.99 eV is relatively weak, the DOS peak at -0.21 eV is quite strong. The quite strong DOS peak at -0.21 eV and the relatively weak DOS peak at 0.99 eV are expected to result in a large value of the joint DOS. As is well known, the absorption intensity of the optical transitions in solids is determined by the joint DOS of the occupied state below Fermi energy and the empty state above Fermi energy,[60] so the two DOS peaks at -0.21 eV and 0.99 eV should lead to a peak-like structure at ~ 1.20 eV in the optical absorption spectra of Nb_3SiTe_6. Thus, the distinct peak-like feature around 1.20 eV in the $\sigma_1(\omega)$ can be assigned as the direct optical transitions between the two flat bands in Nb_3SiTe_6 (see the red vertical arrow in Fig. 2(a)), which host the DOS peaks and are separately located at -0.21 eV and 0.99 eV. Furthermore, the two direct optical transitions between the non-flat bands along the momentum direction S–Y, which are indicated by the yellow vertical arrows in Fig. 2(a), have the energies of ~ 1.20 eV and should contribute to the formation of the peak-like feature around 1.20 eV in the $\sigma_1(\omega)$ as well. However, the DOSs of the non-flat bands related to the direct optical transitions along the direction S–Y should be lower than those of the two flat bands at -0.21 eV and 0.99 eV along the direction Z–U. Therefore, the remarkable peak-like feature around 1.20 eV is mainly contributed by the direct optical transitions between the two flat bands along the momentum direction Z–U. If these two flat bands are separately tuned to be at the Fermi energy

via electron-like and hole-like charge-carrier doping, the DOS at the Fermi energy would be quite high, which may induce superconductivity in this topological hourglass semimetal.[6,8,12] It was previously reported that in Mo_5Si_3, its flat band along X–M originally far away from the Fermi level moves towards the Fermi level after partially replacing the silicon atoms by phosphorus atoms.[12] In $Mo_5Si_{3-x}P_x$ ($x \simeq 1.3$), its flat band with a negligible modification of the energy-momentum dispersions is located at the Fermi level. Meanwhile, their superconducting quantities have been significantly changed. In addition, we have compared the other peak-like features L_2, L_3, L_4, L_6 and L_7 with the calculated band structure and DOS. The peak-like features L_2, L_3, L_4, L_6 and L_7 can be assigned as the optical transitions between the bands with high DOS (see the red vertical arrows in supplemental Figs. 1(a)–1(e)).

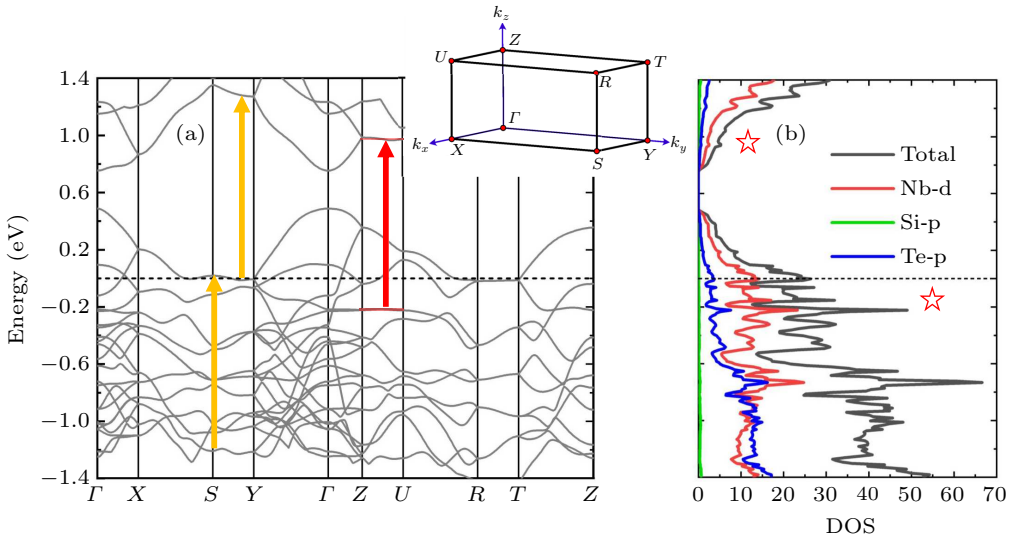


Fig. 2. (a) Electronic band structure of Nb_3SiTe_6 obtained by *ab-initio* calculations. The red vertical arrow indicates the direct optical transitions between the two flat bands. The inset of (a) shows the high symmetry directions of the first Brillouin zone of Nb_3SiTe_6. The first Brillouin zone here corresponds to the in-plane lattice parameters $a = 11.5$ Å, $b = 6.3$ Å, and the lattice parameter along the interlayer direction $c = 13.9$ Å. (b) Total density of states and partial density of states of the electronic bands with Nb 4d, Si 2p and Te 5p orbital characters.

3. Conclusion

In summary, we have studied the nature of the distinct peak-like feature around 1.20 eV in the $\sigma_1(\omega)$ of Nb_3SiTe_6 using optical spectroscopy with the electric field of the incident light parallel to the crystalline *ab*-plane. The peak-like feature around 1.20 eV arises primarily from the direct optical transitions between the two flat bands with the high DOSs and the energy distance ~ 1.20 eV along the momentum direction Z–U and can serve as an optical signature of the flat bands in topological hourglass semimetal Nb_3SiTe_6.

Acknowledgments

Project supported by the Guangdong Basic and Applied Basic Research Foundation (Grant No. 2021B1515130007), the National Natural Science Foundation of China (Grant Nos. U21A20432 and 52273077), the National Key Research and Development Program of China (Grant No. 2022YFA1403800), the Strategic Priority Research Program of Chinese Academy of Sciences (Grant No. XDB33000000), and the Synergetic Extreme Condition User Facility (SECUF, https://cstr.cn/31123.02.SECUF)–Infrared Unit in THz and Infrared Experimental Station.

References

[1] Wang Y F, Gu Z C, Gong C D and Sheng D N 2011 *Phys. Rev. Lett.* **107** 146803
[2] Lu Z, Han T, Yao Y, Reddy A P, Yang J, Seo J, Watanabe K, Taniguchi T, Fu L and Ju L 2024 *Nature* **626** 759
[3] Wang Y F, Yao H, Gong C D and Sheng D N 2012 *Phys. Rev. B* **86** 201101
[4] Zeng T S and Sheng D N 2018 *Phys. Rev. B* **97** 035151
[5] Zhu W, Sheng D N and Haldane F D M 2013 *Phys. Rev. B* **88** 035122
[6] Balents L, Dean C R, Efetov D K and Young A F 2020 *Nat. Phys.* **16** 725
[7] Tian H, Gao X, Zhang Y, Che S, Xu T, Cheung P, Watanabe K, Taniguchi T, Randeria M, Zhang F, Lau C N and Bockrath M W 2023 *Nature* **614** 440
[8] Kauppila V J, Aikebaier F and Heikkilä T T 2016 *Phys. Rev. B* **93** 214505
[9] Iglovikov V I, Hébert F, Grémaud B, Batrouni G G and Scalettar R T 2014 *Phys. Rev. B* **90** 094506
[10] Imada M and Kohno M 2000 *Phys. Rev. Lett.* **84** 143
[11] Hofmann J S, Berg E and Chowdhury D 2023 *Phys. Rev. Lett.* **130** 226001
[12] Khasanov R, Ruan B B, Shi Y Q, Chen G F, Luetkens H, Ren Z A and Guguchia Z 2024 *Nat. Commun.* **15** 2197
[13] Tang E and Fu L 2014 *Nat. Phys.* **10** 964
[14] Su X F, Gu Z L, Dong Z Y, Yu S L and Li J X 2019 *Phys. Rev. B* **99** 014407
[15] Repellin C, Dong Z, Zhang Y H and Senthil T 2020 *Phys. Rev. Lett.* **124** 187601
[16] Kusakabe K and Aoki H 1994 *Phys. Rev. Lett.* **72** 144
[17] Pons R, Mielke A and Stauber T 2020 *Phys. Rev. B* **102** 235101
[18] Arita R, Shimoi Y, Kuroki K and Aoki H 1998 *Phys. Rev. B* **57** 10609
[19] Lin Z, Choi J H, Zhang Q, Qin W, Yi S, Wang P, Li L, Wang Y, Zhang H, Sun Z, Wei L, Zhang S, Guo T, Lu Q, Cho J H, Zeng C and Zhang Z 2018 *Phys. Rev. Lett.* **121** 096401

[20] Li Z, Zhuang J, Wang L, Feng H, Gao Q, Xu X, Hao W, Wang X, Zhang C, Wu K, Dou S X, Chen L, Hu Z and Du Y 2018 *Sci. Adv.* **4** eaau4511

[21] Chen X Z, Wang L, Zhang S, Zhang R J, Cheng Y W, Hu Y D, Meng C N, Liu Z T, Lv B Q and Huang Y B 2024 *Chin. Phys. B* **33** 087402

[22] Ye J, Lin Y, Wang H, Song Z, Feng J, Xie W and Jia S 2024 *Chin. Phys. B* **33** 057103

[23] Kang M, Fang S, Ye L, Po H C, Denlinger J, Jozwiak C, Bostwick A, Rotenberg E, Kaxiras E, Checkelsky J G and Comin R 2020 *Nat. Commun.* **11** 4004

[24] Okamoto S, Mohanta N, Dagotto E and Sheng D N 2022 *Commun. Phys.* **5** 198

[25] Kang M, Ye L, Fang S, *et al*. 2020 *Nat. Mater.* **19** 163

[26] Liu Z, Li M, Wang Q, Wang G, Wen C, Jiang K, Lu X, Yan S, Huang Y, Shen D, Yin J X, Wang Z, Yin Z, Lei H and Wang S 2020 *Nat. Commun.* **11** 4002

[27] Yin J X, Zhang S S, Chang G, *et al*. 2019 *Nat. Phys.* **15** 443

[28] Li M, Wang Q, Wang G, Yuan Z, Song W, Lou R, Liu Z, Huang Y, Liu Z, Lei H, Yin Z and Wang S 2021 *Nat. Commun.* **12** 3129

[29] Di Sante D, Bigi C, Eck P, Enzner S, Consiglio A, Pokharel G, Carrara P, Orgiani P, Polewczyk V, Fujii J, King P D C, Vobornik I, Rossi G, Zeljkovic I, Wilson S D, Thomale R, Sangiovanni G, Panaccione G and Mazzola F 2023 *Nat. Phys.* **19** 1135

[30] Zhang H, Shi Z, Jiang Z, Yang M, Zhang J, Meng Z, Hu T, Liu F, Cheng L, Xie Y, Zhuang J, Feng H, Hao W, Shen D and Du Y 2023 *Adv. Mater.* **35** 2301790

[31] Han M, Inoue H, Fang S, John C, Ye L, Chan M K, Graf D, Suzuki T, Ghimire M P, Cho W J, Kaxiras E and Checkelsky J G 2021 *Nat. Commun.* **12** 5345

[32] Jiang Z, Liu Z, Ma H, Xia W, Liu Z, Liu J, Cho S, Yang Y, Ding J, Liu J, Huang Z, Qiao Y, Shen J, Jing W, Liu X, Liu J, Guo Y and Shen D 2023 *Nat. Commun.* **14** 4892

[33] Sun Z, Zhou H, Wang C, Kumar S, Geng D, Yue S, Han X, Haraguchi Y, Shimada K, Cheng P, Chen L, Shi Y, Wu K, Meng S and Feng B 2022 *Nano Lett.* **22** 4596

[34] Huang H, Zheng L, Lin Z, Guo X, Wang S, Zhang S, Zhang C, Sun Z, Wang Z, Weng H, Li L, Wu T, Chen X and Zeng C 2022 *Phys. Rev. Lett.* **128** 096601

[35] Ye L, Fang S, Kang M, Kaufmann J, Lee Y, John C, Neves P M, Zhao S Y F, Denlinger J, Jozwiak C, Bostwick A, Rotenberg E, Kaxiras E, Bell D C, Janson O, Comin R and Checkelsky J G 2024 *Nat. Phys.* **20** 610

[36] Ghimire N J and Mazin I I 2020 *Nat. Mater.* **19** 137

[37] Yang J, Yi X, Zhao Z, *et al*. 2023 *Nat. Commun.* **14** 4089

[38] Multer D, Yin J X, Hossain M S, Yang X, Sales B C, Miao H, Meier W R, Jiang Y X, Xie Y, Dai P, Liu J, Deng H, Lei H, Lian B and Zahid Hasan M 2023 *Commun. Mater.* **4** 17

[39] Peng S, Han Y, Pokharel G, Shen J, Li Z, Hashimoto M, Lu D, Ortiz B R, Luo Y, Li H, Guo M, Wang B, Cui S, Sun Z, Qiao Z, Wilson S D and He J 2021 *Phys. Rev. Lett.* **127** 266401

[40] Xing S, Zhao T, Zhou J and Sun Z 2024 *J. Phys. Chem. C* **128** 2618

[41] Regmi S, Fernando T, Zhao Y, Sakhya A P, Dhakal G, Bin Elius I, Vazquez H, Denlinger J D, Yang J, Chu J H, Xu X, Cao T and Neupane M 2022 *Commun. Mater.* **3** 100

[42] Lisi S, Lu X, Benschop T, *et al*. 2021 *Nat. Phys.* **17** 189

[43] Lu B, Yada K, Sato M and Tanaka Y 2015 *Phys. Rev. Lett.* **114** 096804

[44] Chen A and Franz M 2016 *Phys. Rev. B* **93** 201105

[45] Zhou Y, Jin K H, Huang H, Wang Z and Liu F 2019 *Phys. Rev. B* **99** 201105

[46] Zyuzin A A and Zyuzin A Y 2018 *Phys. Rev. B* **97** 041203

[47] Utama M I B, Koch R J, Lee K, Leconte N, Li H, Zhao S, Jiang L, Zhu J, Watanabe K, Taniguchi T, Ashby P D, Weber Bargioni A, Zettl A, Jozwiak C, Jung J, Rotenberg E, Bostwick A and Wang F 2021 *Nat. Phys.* **17** 184

[48] Ma N, Wang D Y, Huang B R, Li K Y, Song J P, Liu J Z, Mei H P, Ye M and Li A 2023 *Chin. Phys. B* **32** 056801

[49] Liu H, Cao Y, Xu Y, Gawryluk D J, Pomjakushina E, Gao S Y, Dudin P, Shi M, Yan L, Yang Y f and Ding H 2020 *Phys. Rev. B* **102** 035111

[50] Song Z D and Bernevig B A 2022 *Phys. Rev. Lett.* **129** 047601

[51] Li S, Liu Y, Wang S S, Yu Z M, Guan S, Sheng X L, Yao Y and Yang S A 2018 *Phys. Rev. B* **97** 045131

[52] Liu R Y, Huang A, Sankar R, Hlevyack J A, Su C C, Weng S C, Lin M K, Chen P, Cheng C M, Denlinger J D, Mo S K, Fedorov A V, Chang C S, Jeng H T, Chuang T M and Chiang T C 2023 *Nano Lett.* **23** 380

[53] Liu Z, Li T, Zhang B, Adam M L, Zhu W, Li Y, Wang S, Wu Y, Zhu H, Cao D, Cui Q, Cui S, Liu Y, Chen S, Sun Z and Song L 2022 *iScience* **25**

[54] Wan Q, Yang T Y, Li S, *et al*. 2021 *Phys. Rev. B* **103** 165107

[55] Hu J, Liu X, Yue C L, Liu J Y, Zhu H W, He J B, Wei J, Mao Z Q, Antipina L Y, Popov Z I, Sorokin P B, Liu T J, Adams P W, Radmanesh S M A, Spinu L, Ji H and Natelson D 2015 *Nat. Phys.* **11** 471

[56] An L, Zhang H, Hu J, Zhu X, Gao W, Zhang J, Xi C, Ning W, Mao Z and Tian M 2018 *Phys. Rev. B* **97** 235133

[57] Zhao Y, Cao J, Zhang Z, Li S, Li Y, Ma F and Yang S A 2023 *Phys. Rev. B* **107** 205124

[58] Pang Y, Rezaei E, Chen D, Li S, Jian Y, Wang Q, Wang Z, Duan J, Zebarjadi M and Yao Y 2020 *Phys. Rev. Mater.* **4** 094205

[59] Ebad Allah J, Tsirlin A A, Zhu Y L, Mao Z Q and Kuntscher C A 2023 *Phys. Rev. B* **107** 115115

[60] Dressel M and Grüner G 2002 *Electrodynamics of solids: optical properties of electrons in matter* (Cambridge University Press)

[61] Xu Y, Zhao J, Yi C, Wang Q, Yin Q, Wang Y, Hu X, Wang L, Liu E, Xu G, Lu L, Soluyanov A A, Lei H, Shi Y, Luo J G and Chen Z G 2020 *Nat. Commun.* **11** 3985

[62] Hu W Z, Dong J, Li G, Li Z, Zheng P, Chen G F, Luo J L and Wang N L 2008 *Phys. Rev. Lett.* **101** 257005

[63] Mirri C, Dusza A, Bastelberger S, Chinotti M, Degiorgi L, Chu J H, Kuo H H and Fisher I R 2015 *Phys. Rev. Lett.* **115** 107001

[64] Nakajima M, Liang T, Ishida S, Tomioka Y, Kihou K, Lee C H, Iyo A, Eisaki H, Kakeshita T, Ito T and Uchida S 2011 *Proc. Natl. Acad. Sci. USA* **108** 12238

[65] Moskalenko S A E and Snoke D W 2000 *Bose-Einstein condensation of excitons and biexcitons: and coherent nonlinear optics with excitons* (Cambridge University Press)

[66] Klingshirn C F 2012 *Semiconductor optics* (Springer Science & Business Media)

[67] Mott N F 1968 *Rev. Mod. Phys.* **40** 677

[68] Mahan G D 1967 *Phys. Rev. Lett.* **18** 448

[69] Mahan G D 1967 *Phys. Rev.* **153** 882

[70] Xu Y, Wang J, Su B, Deng J, Peng C, Wu C, Zhang Q, Gu L, Luo J, Xu N, Guo J and Chen Z G 2023 *Commun. Mater.* **4** 69

[71] Landau L D 1933 *Phys. Z. Sowjet.* **3** 664

[72] Devreese J T and Alexandrov A S 2009 *Reports on Progress in Physics* **72** 066501

[73] Fujioka J, Yamada R, Okawa T and Tokura Y 2021 *Phys. Rev. B* **103** L041109